



A general theory of ignition and combustion of nano- and micron-sized aluminum particles



Dilip Srinivas Sundaram^{a,*}, Puneesh Puri^{b,1}, Vigor Yang^{a,**}

^aSchool of Aerospace Engineering, Georgia Institute of Technology, Atlanta, GA 30332, USA

^bDepartment of Mechanical and Nuclear Engineering, The Pennsylvania State University, University Park, PA 16802, USA

ARTICLE INFO

Article history:

Received 9 August 2015

Revised 2 April 2016

Accepted 5 April 2016

Available online 8 May 2016

Keywords:

Aluminum

Ignition

Combustion

Burning time

Particle size

Flame temperature

ABSTRACT

A general theory of ignition and combustion of nano- and micron-sized aluminum particles is developed. The oxidation process is divided into several stages based on phase transformations and chemical reactions. Characteristic time scales of different processes are compared to identify physicochemical phenomena in each stage. In the first stage, the particle is heated to the melting temperature of the aluminum core. Key processes are heat and mass transfer between the gas and particle surface and diffusion of mass and energy inside the particle. The second stage begins upon melting of the aluminum core. Melting results in pressure buildup, thereby facilitating mass diffusion and/or cracking of the oxide layer. Melting is followed by polymorphic phase transformations, which also results in the formation of openings in the oxide layer. These provide pathways for the molten aluminum to react with the oxidizing gas; the ensuing energy release results in ignition of nano-aluminum particles. For large micron-sized particles, ignition is not achieved due to their greater volumetric heat capacity. In the third stage, nanoparticles undergo vigorous self-sustaining reactions with the oxidizing gas. Reactions typically occur heterogeneously in the particle and the burning rate is controlled by chemical kinetics. For large micron-sized particles, polymorphic phase transformations result in the formation of a crystalline oxide layer. The oxide layer melts and particle ignition is achieved. In the fourth stage, the large micron-sized particle burns through gas-phase or surface reactions, depending on the oxidizer and pressure. The burning rate is controlled by mass diffusion through the gas-phase mixture.

© 2016 The Combustion Institute. Published by Elsevier Inc. All rights reserved.

1. Introduction

Metal particles are attractive fuel candidates for various propulsion and energy-conversion applications. Of all metals, aluminum is popular because of its high energy density, relative safety, and low cost [1]. The enthalpy of combustion of aluminum particles in oxygen at stoichiometric conditions is 84 kJ/cm³, substantially greater than those of monomolecular energetic materials such as trinitrotoluene (~10–30 kJ/cm³). Nascent aluminum particles are pyrophoric and react spontaneously in any oxidizing environment [2]. As a result, particles are passivated by exposing them to an oxidizing gas in a well-controlled manner. This results in the formation of an amorphous oxide (Al₂O₃) layer of thickness in the range of 2–4 nm [3,4]. For micron-sized and larger particles, ignition is

commonly associated with melting of the oxide layer at 2350 K [5]. The molten oxide shell forms a cap on the particle surface under the effect of surface tension, thereby exposing the aluminum core to the oxidizing gas. The high ignition temperature and particle agglomeration diminish energy-release rates in various practical applications.

Nanomaterials have unique and favorable physicochemical properties owing to the presence of large percentage of atoms on the surface. The percentage of atoms on the surface layer of an aluminum particle increases from 2% to 92%, when the particle size decreases from 100 to 1 nm. Surface atoms have higher energy than the atoms in interior regions of the particle. As a result, properties are size-dependent and substantially different from those of bulk materials.

Figure 1 shows the effect of particle size on the ignition temperature of aluminum particles [6]. Experimental data are taken from Refs. [5,7–21]. The ignition temperature of aluminum particles decreases with decreasing particle size, from about 2350 K at 100 μm to about 1000 K at 100 nm. Note that there is a considerable scatter in the experimental data owing to differences in experimental conditions including apparatus, sample type, heating

* Corresponding author. Present address: Indian Institute of Technology Gandhinagar, Palaj, Gujarat 382355, India.

** Corresponding author. Fax: +1 404 894 2760.

E-mail addresses: dilip.sundaram@iitgn.ac.in (D.S. Sundaram),

vigor.yang@aerospace.gatech.edu (V. Yang).

¹ Present address: Intel Corporation, Bengaluru, India.

Nomenclature

| | |
|-----------|--|
| a | distance between energy barrier maximum and adjacent minimum |
| A | surface area |
| B | transfer number |
| Bi | Biot number |
| c | molecular speed |
| C | concentration |
| C_p | constant-pressure specific heat |
| C_v | constant-volume specific heat |
| D | diameter, diffusivity |
| E_A | activation energy |
| h | heat transfer coefficient |
| h_m | latent heat of melting |
| h_r | heat of reaction |
| H_{vap} | heat of vaporization |
| i | stoichiometric fuel-oxidant mass ratio |
| K | bulk modulus |
| k | chemical rate constant |
| k_B | Boltzmann constant |
| Kn | Knudsen number |
| L_v | latent heat of vaporization |
| m | mass |
| M | molecular weight |
| M_p | particle mass |
| n | number of ions per unit area |
| N_A | Avogadro's number |
| p | pressure |
| Pr | Prandtl number |
| \dot{q} | energy per unit time |
| Q_r | heat of reaction |
| R | particle radius, gas constant |
| Re | Reynolds number |
| T | temperature |
| t | time |
| V | velocity, volume |
| W | energy barrier |
| X | mole fraction |
| Y | mass fraction |

Greek letters

| | |
|---------------|-----------------------------------|
| β | Knudsen layer thickness |
| λ | thermal conductivity |
| τ | time |
| μ | viscosity |
| α | energy accommodation coefficient |
| γ | adiabatic constant |
| θ | Debye temperature |
| ρ | density |
| ε | emissivity |
| δ | oxide layer thickness |
| σ | stress, Stefan-Boltzmann constant |
| Ω | volume per displaced ion |
| ν | attempt frequency |
| ϕ | Mott potential |

Subscripts

| | |
|----------|----------------|
| θ | azimuthal |
| ϕ | polar |
| a | ambient gas |
| am | amorphous |
| b | burn |
| c | critical, core |

| | |
|--------------------|----------------------------------|
| <i>cond</i> | conduction |
| <i>diff</i> | diffusion |
| <i>frac</i> | fracture |
| <i>gen</i> | generation |
| <i>heat</i> | heating |
| <i>melt</i> | melting |
| <i>O</i> | oxidizer |
| <i>ox</i> | oxide |
| <i>p</i> | particle |
| <i>poly</i> | polymorphic phase transformation |
| <i>r</i> | radial |
| <i>rad</i> | radiation |
| Superscript | |
| <i>tr</i> | transformation |

rate, oxide layer thickness and purity, and oxidizer composition. Care must therefore be taken when comparing data from different experiments. For example, Friedman et al.'s data [5] suggest that ignition temperatures of micron-sized aluminum particles are relatively near the melting point of the oxide film and are not a strong function of particle size. Results of Gurevich et al.'s experiments [15], on the other hand, indicate that ignition temperatures of micron-sized particles are substantially lower than the oxide melting point and decreases significantly with increasing oxidizer concentration. Khaikin et al. [22] proposed that particle ignition in experiments of Friedman et al. [5] is due to particle heating to the melting point of the oxide film, while the trends obtained by Gurevich et al. [15] was explained by considering the crystallization of the oxide layer and thermal inertia of particles. Furthermore, particle impurity (presence of magnesium in the particle) also affects the ignition temperature. As MgO is a non-protective oxide layer, ignition may occur at temperatures lower than the core melting point, as observed by Bulian et al. [10].

Nonetheless, it is apparent that nanoaluminum particles ignite at temperatures as low as ~ 1000 K, substantially lower than the bulk melting point of the oxide shell (2350 K). This phenomenon has been attributed to cracking of the oxide layer due melting of the aluminum core [23] and polymorphic phase transformations in the oxide layer [4]. Upon melting, the density of the aluminum core decreases from 2700 to 2400 kg/m³, an 11.1% change. The molten aluminum core thus exerts tensile stresses and could fracture the oxide layer. The cracks provide pathways for the oxidizing gas to react with the aluminum core. The ensuing energy release results in ignition of nanoaluminum particles. For micron-sized and larger particles, the energy release is insufficient

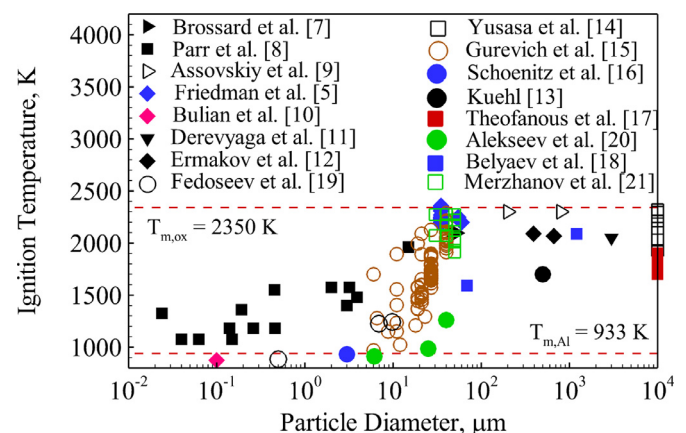


Fig. 1. Effect of particle size on ignition temperature of aluminum particles (adapted from Ref. [6]).

Table 1
Adiabatic flame temperatures of aluminum particles for different oxidizers at 1 atm pressure.

| Reactants | Adiabatic flame temperature (K) |
|---|---------------------------------|
| 2Al(s)+1.5O ₂ | 3977.0 |
| 2Al(s)+1.5(O ₂ +3.76N ₂) | 3546.5 |
| 2Al(s)+3H ₂ O | 3052.8 |
| 2Al(s)+3CO ₂ | 3144.4 |
| 2Al(s)+3CO | 2277.2 |

to ignite these particles due to their higher volumetric heat capacity; ignition is thus achieved at temperatures as high as the melting temperature of the oxide shell (2350 K).

The ignition mechanism of nanoaluminum particles remains an unsettled problem. Rai et al. [23] studied the thermomechanical and oxidation behaviors of nanoaluminum particles using hot-stage transmission electron microscopy (TEM) and single-particle mass spectrometer over a temperature range of 293–1173 K. Particles with an oxide layer thickness of about 3 nm and diameters in the range of 20–30 nm were considered. Images of particles heated in a hot-stage TEM suggest that the oxide layer cracked upon melting of the aluminum core. The tensile stress in the oxide layer was estimated to be on the order of 10 GPa, significantly greater than the measured tensile strength of alumina (0.25 GPa at 298 K [24]). It was thus proposed that ignition of nano-aluminum particles is caused by melting of the aluminum core. Trunov et al. [4], on the other hand, attributed ignition of nano-aluminum particles to polymorphic phase transformations in the oxide layer. In their study, oxidation of 3–14 μm aluminum powders was studied using thermogravimetric analysis. The powders were heated in oxygen up to 1500 °C at heating rates on the order of 10 K/min. Aluminum oxide exists in different forms; the three major polymorphs of concern are amorphous, gamma, and alpha alumina. At about 550 °C, the amorphous oxide layer transforms into gamma alumina. The density of gamma alumina is 3660 kg/m³, greater than that of amorphous polymorph (3050 kg/m³) [4]. As a result, the newly formed oxide layer does not completely cover the particle surface, thereby facilitating ignition of nanoaluminum particles. It is unclear if ignition of nanoaluminum particles is triggered by core melting or polymorphic phase transformations in the oxide layer.

The combustion of micron-sized and larger aluminum particles has been studied extensively. Upon ignition, chemical reactions can occur homogeneously in the gas-phase or heterogeneously at the particle surface. The mode of combustion depends on the composition of the oxidizer. Table 1 shows the adiabatic flame temperatures of aluminum particles for different oxidizers at 1 atm pressure. With the exception of carbon monoxide, the adiabatic flame temperature is greater than the boiling point of aluminum (2700 K). As a result, vapor-phase reactions occur in most oxidizers at 1 atm pressure. Pressure is yet another parameter that dictates the mode of combustion. The flame temperature is a pressure-dependent parameter and is typically greater than the boiling point of aluminum for pressures lower than a threshold value. For water vapor and carbon dioxide, the threshold pressure is ~5 atm. Combustion of aluminum particles in water and carbon dioxide occur heterogeneously at the particle surface for pressures exceeding 5 atm. Homogenous gas-phase reactions typically occur for oxygen and air, since the flame temperature is greater than the boiling point of aluminum over a broad pressure range of about 1–100 atm.

The burning behavior of micron-sized aluminum particles is well understood. The measured flame temperatures are approximately equal to the adiabatic counterparts [25–27]. The combustion of micron-sized aluminum particles in air can be divided into two stages [27,28]. In the first stage, the particle is surrounded by a detached vapor-phase flame and undergoes steady and symmet-

ric combustion. As alumina decomposes during volatilization, gas-phase sub-oxides (AlO and AlO₂) are formed. The dissolution of gas-phase sub oxides in the liquid droplet marks the onset of the second stage. The second stage is characterized by unsteady and asymmetric combustion, spinning of particles and/or oxide smoke, and ejections of gas-phase sub-oxides from the particle surface. Detailed discussions on the combustion characteristics of micron-sized aluminum particles can be found in Refs. [27] and [28]. The flame standoff ratio (D_f/D_p) is 2.0–3.0 in oxygenated environments, but is as low as 1.3 in water vapor [29]. For aluminum particles with diameters greater than 20 μm, the burning time is given by [30]

$$t_b = \frac{cD_p^{1.8}}{X_{eff}p^{0.1}T_0^{0.2}}, \quad (1)$$

where X_{eff} is the effective oxidizer concentration, $X_{eff} = C_{O_2} + 0.6C_{H_2O} + 0.22C_{CO_2}$, p the pressure in atm, T_0 the initial temperature in Kelvin, D_p the particle diameter in μm, and c a constant ($= 7.35 \times 10^{-6}$). The burning time is quadratically proportional to particle size and is weakly dependent on the temperature and pressure of the gas. These suggest that the particle burning rate is controlled by mass diffusion phenomena.

The combustion characteristics of nanoaluminum particles are substantially different from those of micron-sized counterparts. Bazyn et al. [31] studied the combustion of 80 nm aluminum particles in oxygen–nitrogen gas mixture using a shock tube. The gas temperature varied in the range of 1200–2100 K and the pressure range of concern was 4–32 atm. The flame temperature was measured using pyrometry and the burning time was inferred based on the temporal variation of the intensity of light emitted by the particles. The measured flame temperatures were substantially lower than the adiabatic counterparts. For example, at a pressure of 4 atm, the flame temperatures of 80 nm particles were as low as the ambient gas temperature (1200–2100 K). The burning time was an exponential function of the gas temperature; the activation energy was estimated to be 71.6 and 50.6 kJ/mol at 8 and 32 atm, respectively. Gas pressure exerted a strong effect on the burning time of nano-aluminum particles. For example, at a temperature of ~1400 K, the burning time decreased by a factor of four when the pressure increased from 4 to 32 atm. At nano-scales, the burning time has a particle size dependence of the form, $t_b \sim a D_p^n$, where the exponent n is as low as 0.3 [32]. It was speculated that the particle burning rate is controlled by chemical kinetics or mass diffusion across the oxide layers of the particles [31].

Park et al. [33] studied the oxidation of nanoaluminum particles in air using single particle mass spectrometer for temperatures up to 1373 K at low heating rates ($< 10^3$ K/s). The particle size range of concern was 50–150 nm. The oxidation rate was controlled by mass diffusion across the oxide layer of the particle rather than chemical kinetics. Furthermore, the particles did not burn completely even after 15 s. These observations contradict those of Bazyn et al. [31] obtained at higher heating rates (10^6 – 10^8 K/s) in a shock tube. The measured burning times of Bazyn et al. were on the order of 100 μs [31]. It is unclear if chemical kinetics or mass diffusion controls the burning rate of nano-aluminum particles. The combustion mode and flame structures of nano-aluminum particles need careful examination as well.

In view of the uncertainties and conflicting notions in existing theories, development of a general theory accommodating various underlying physicochemical processes over a broad range of particle sizes is much needed. In the present study, the oxidation of aluminum particles in different stages is examined systematically. Key phenomena in each stage are identified based on their respective time scales. Special effort is applied to consolidate observations and findings from different perspectives and establish a

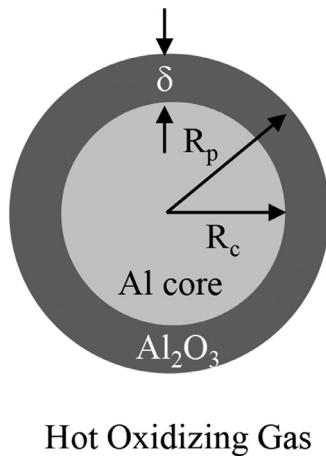


Fig. 2. Physical model of concern – a passivated aluminum particle in a hot oxidizing gas.

unified theory of ignition and combustion of nano- and micron-sized aluminum particles.

2. General theory on oxidation of aluminum particles

The physical model of concern is a passivated aluminum particle in a hot oxidizing gas, as shown in Fig. 2. The aluminum particle is covered by an amorphous oxide layer of thickness in the range of 2–4 nm [3, 4]. The ambient gas temperature, T_a , is taken to be equal to or greater than the minimum ignition temperature of the particle, T_{ign} . Table 2 shows the physicochemical properties of aluminum and aluminum oxide. The properties of the particle are size-dependent, especially for diameters lower than 10 nm. The melting temperature of aluminum core increases with increasing particle size, from 473 K at 2 nm to 933 K at 10 nm [34]. A similar trend is observed for the oxide shell [35]. For aluminum particles in the size range of 5–10 nm, the melting temperature of the oxide shell is in the range of 986–1313 K over a shell-thickness range of 0.5–2.0 nm. Note that these values are substantially lower than the bulk melting point of 2350 K. The enthalpy of oxidation of aluminum is also a function of particle size, decreasing from ~1690 kJ/mol at 10 nm to 824 kJ/mol at 2 nm [36]. This was obtained by considering size dependencies of the cohesive energy of aluminum and lattice energy of aluminum oxide. The trend however needs to be verified experimentally. The ignition temperature is size-dependent for particles smaller than 100 μm . It decreases with decreasing particle size, from 2350 K at 100 μm to 1000 K at 100 nm.

Table 2
Physicochemical properties of aluminum and aluminum oxide.

| Material | Al | Al ₂ O ₃ | Remarks |
|---|-----------------------|---|--|
| Density (kg/m ³) | 2700 (s) ^a | 3050 (am) ^a 3660 (γ) ^a 3900 (α) ^a 3010 (l) ^b | Al ₂ O ₃ can exist in five different forms |
| Specific heat (J/kg K) ^a | 897 | 718 | – |
| Melting point (K) | 448–933 [34] | 1000–2350 [35] | Size dependent for $D_p < 10$ nm |
| Boiling point (K) ^c | 2740 | 4000 | – |
| Thermal conductivity (W/m K) ^a | 205 | 30 | – |
| Ignition temperature (K) | 933–2350 [6] | – | Size dependent for $D_p < 100$ μm |
| Heat of reaction (kJ/mol) ^d | 824–1690 [36] | – | Size dependent for $D_p < 10$ nm |

^a 298 K.

^b Melting temperature.

^c 1 atm pressure.

^d $2\text{Al} + 1.5\text{O}_2 \rightarrow \text{Al}_2\text{O}_3$.

The oxidation of aluminum particles can be divided into different stages based on phase transformations and chemical reactions. Figures 3 and 4 show the stages of oxidation of nano- and large micron-sized aluminum particles, respectively. In the first stage, the particle is heated to the melting temperature of the aluminum core. Key processes are heat and mass transfer between the gas and particle surface and diffusion of mass and energy inside the particle. The second stage begins upon melting of the aluminum core. Melting results in pressure buildup and facilitates outward motion of molten aluminum by diffusion and/or flow through the cracks in the oxide layer. Melting is followed by polymorphic phase transformations, which also results in the formation of openings in the oxide layer. The molten aluminum reacts with the oxidizing gas and the ensuing energy release results in ignition of nano-aluminum particles. For large micron-sized particles, ignition is not achieved due to their greater volumetric heat capacity. In the third stage, nanoparticles undergo vigorous self-sustaining reactions with the oxidizing gas. Reactions typically occur heterogeneously in the particle and the burning rate is limited by chemical kinetics. For large micron-sized particles, polymorphic phase transformations result in the formation of a crystalline oxide layer. The oxide layer melts and particle ignition is achieved. In the fourth stage, the large micron-sized particle burns through gas-phase or surface reactions, depending on the oxidizer and pressure. In following sections, key physicochemical processes in each stage are analyzed in detail.

2.1. Stage 1 – particle heating to core melting point

In the first stage, the particle is heated to the melting temperature of the aluminum core. Key processes of concern are energy and mass transfer between gas and particle surface, diffusion of mass and energy inside the particle, and polymorphic phase transformations in the oxide layer.

2.1.1. Heat and mass transfer regimes

Two important length scales of concern are the particle size and mean free path of the gas molecules. The continuum assumption is typically valid when the particle size is substantially greater than the mean free path of the gas molecules. At nano scales, particle size is comparable to the mean free path and the gas cannot be treated as a continuous medium. The Knudsen number, Kn , often used to characterize the situation, defined as the ratio of the mean free path of the gas molecules to the particle size

$$Kn = \frac{RT}{\sqrt{2}\pi D_a^2 N_A p D_p} \quad (2)$$

where R is the gas constant, T the temperature, D_a the diameter of the ambient gas molecule, N_A the Avogadro's number, p the

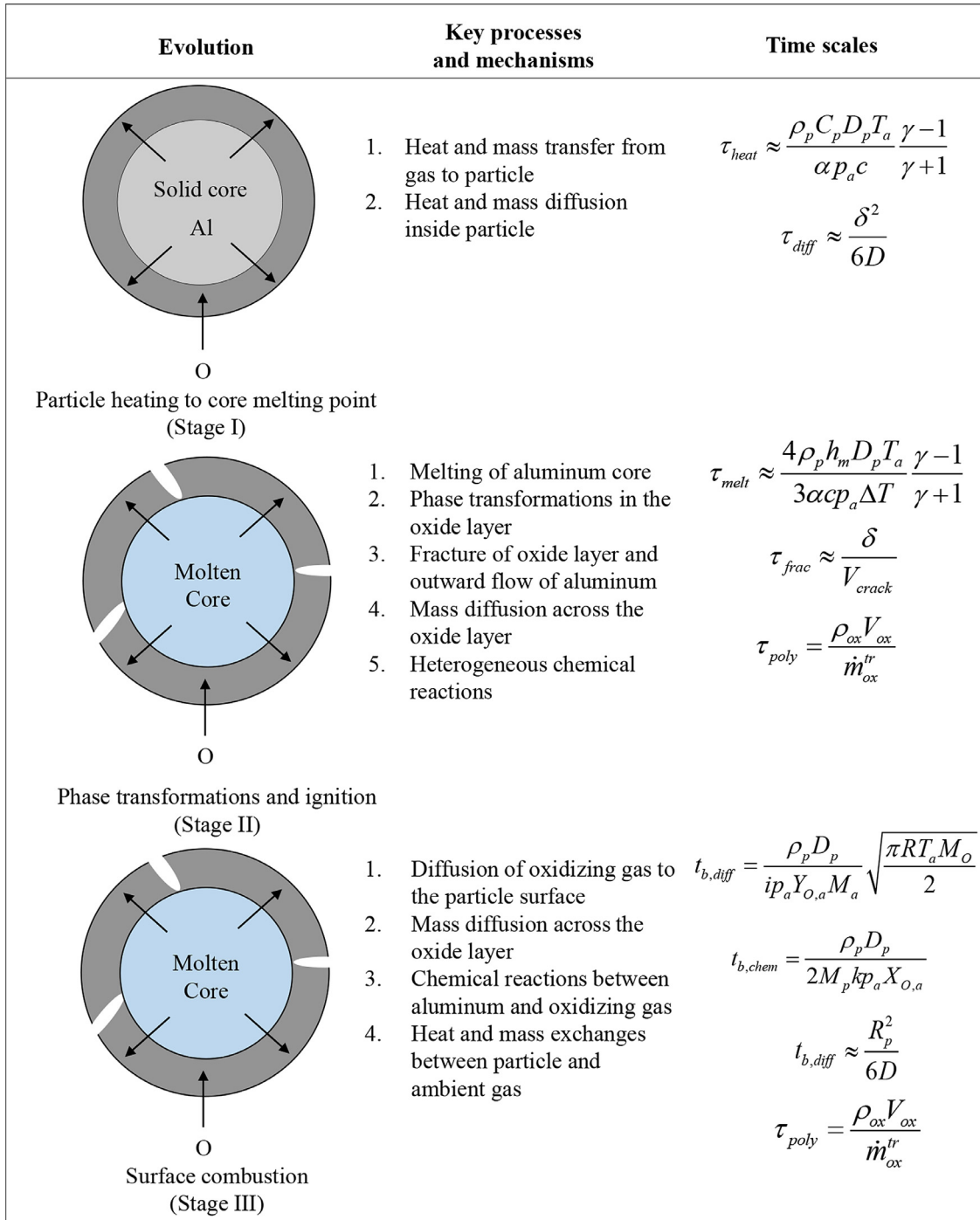


Fig. 3. Three stages of oxidation of nanoaluminum particles.

pressure, and D_p the particle diameter. The continuum hypothesis breaks down for $Kn > 0.01$ and the free-molecular regime prevails for $Kn > 10$ [37]. Figure 5 shows the particle diameters corresponding to the Knudsen numbers of 0.01 and 10 as a function of gas temperature for three different pressures of 1, 10, and 100 atm. At a pressure of 1 atm and temperature of 3000 K, the critical particle size at which continuum approximation ceases to be valid is 70 μm . It decreases by a factor of 10 when the pressure increases from 1 to 10 atm and temperature decreases from 3000 to 300 K. It is apparent that continuum models are not adequate to characterize the ignition and combustion characteristics of nanoaluminum particles.

2.1.2. Heat transfer between particle and gas

The duration of the first stage is the time taken for the particle to be heated to the melting temperature of the aluminum core. The heating process involves two steps: (1) energy transfer from the ambient gas to the particle surface; and (2) diffusion of energy inside the particle. The rate-controlling step can be determined by calculating the Biot number, Bi , [38]

$$Bi = \frac{hD_p}{6\lambda_p}, \quad (3)$$

$$h = \frac{\lambda_a}{D_p} \left[2 + \left(0.4 \text{Re}_{D_p}^{1/2} + 0.06 \text{Re}_{D_p}^{2/3} \right) \text{Pr}^{0.4} \left(\mu_{T_a} / \mu_{T_p} \right)^{1/4} \right], \quad (4)$$

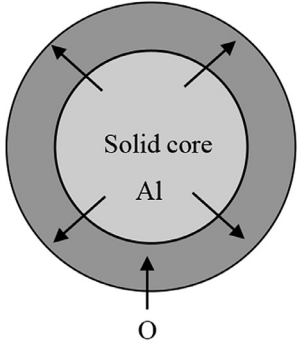
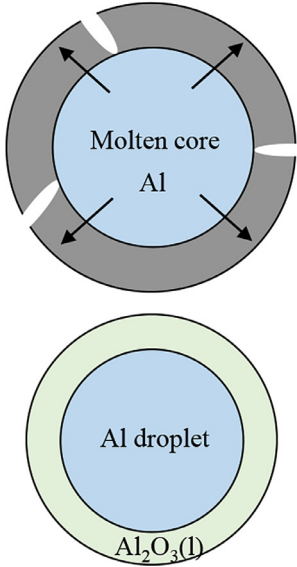
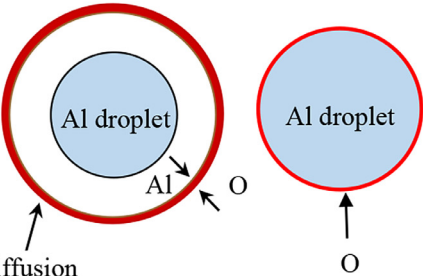
| Evolution | Key processes and mechanisms | Time scales |
|--|--|--|
|  <p data-bbox="288 651 691 715">Particle heating to core melting point (Stage I)</p> | <ol style="list-style-type: none"> 1. Heat and mass transfer from gas to particle 2. Heat and mass diffusion inside particle | $\tau_{heat} \approx \frac{\rho_p C_p D_p^2}{45\lambda_a}$ $\tau_{diff} \approx \frac{\delta^2}{6D}$ |
|  <p data-bbox="288 1347 691 1410">Phase transformations and ignition (Stages II and III)</p> | <ol style="list-style-type: none"> 1. Melting of aluminum core 2. Phase transformations in the oxide layer 3. Cracking of oxide layer and outward flow of aluminum 4. Mass diffusion across the oxide layer 5. Heterogeneous chemical reactions | $\tau_{poly} = \frac{\rho_{ox} V_{ox}}{\dot{m}_{ox}^{tr}}$ $\tau_{frac} \approx \frac{\delta}{V_{crack}}$ $\tau_{melt} \approx \frac{\rho_p h_m D_p^2}{12\lambda_a (T_a - T_m)}$ |
|  <p data-bbox="252 1747 691 1874">Vapor-phase or surface combustion (Stage IV)</p> | <ol style="list-style-type: none"> 1. Diffusion of oxidizing gas and aluminum vapor to the flame zone 2. Chemical reactions between aluminum and oxidizing gas in the flame zone 3. Heat transfer from the flame zone to particle and gas | $t_{b,chem} = \frac{\rho_p D_p}{2M_p k p_a X_{O,a}}$ $t_{b,diff} = \frac{\rho_p D_p^2}{8\rho_a D \log(1+B)}$ |

Fig. 4. Four stages of oxidation of large micron-sized aluminum particles.

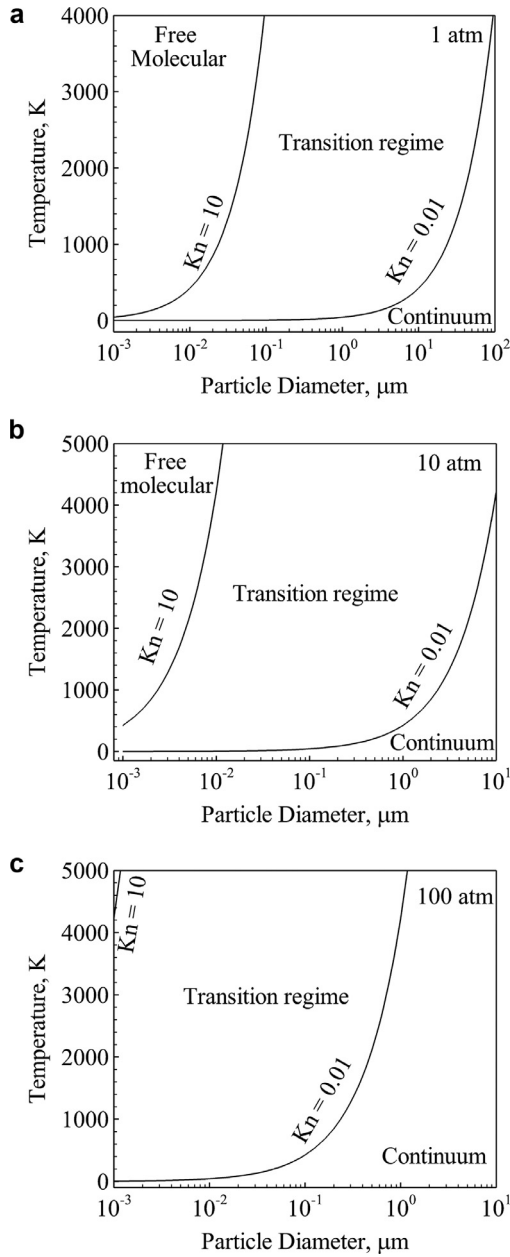


Fig. 5. Particle diameters corresponding to Knudsen numbers of 0.01 and 10 as a function of temperature for three different pressures of 1, 10, and 100 atm.

where h is the heat transfer coefficient, λ the thermal conductivity, Re_{Dp} the Reynolds number based on the particle diameter, Pr the Prandtl number, and μ the viscosity. The subscripts p and a refer to the particle and ambient gas, respectively. The Biot number is the ratio of the heat transfer resistance inside the particle to the counterpart at the particle surface. Figure 6 shows the effect of particle size on the Biot number of aluminum particles in air for different gas velocities. The temperatures of particle and gas are 300 and 1000 K, respectively. For the particle size range of concern, the calculated Biot numbers are orders of magnitude lower than unity. As a result, resistance to energy diffusion inside the particle is negligibly small compared to the surface heat-transfer resistance. Temperature gradients inside the particle are thus negligible and the particle can be assumed to be in thermal equilibrium internally. This is more so should free-molecular effects be considered, since the resulting heat transfer coefficient is lower than the continuum counterpart [39]. Furthermore, inclusion of radiation heat transfer does

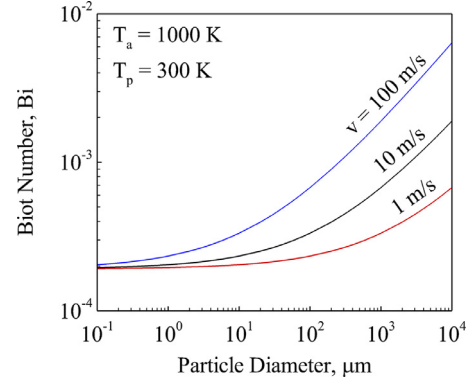


Fig. 6. Biot number of aluminum particles as a function of particle size for different gas velocities.

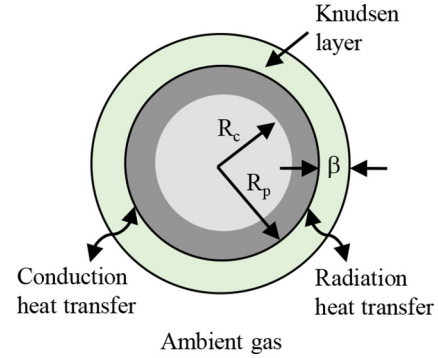


Fig. 7. Heat transfer between particle and ambient gas.

not change the result of the analysis. The particle can be treated as a lumped system and a single temperature variable is sufficient to analyze its ignition and combustion properties.

It is apparent that the heating time is dictated by energy transfer between the gas and particle surface. Figure 7 shows the particle-gas energy exchange mechanism. Heat transfer between the particle and ambient gas occurs by conduction and radiation. Following Fuch's approach [40], the gas volume is divided into two regions: (1) the Knudsen layer in which collisions between gas molecules are negligible; (2) the region outside the Knudsen layer in which molecular collisions are significant. Free-molecular effects are thus confined to the Knudsen layer and continuum laws govern physicochemical processes outside the Knudsen layer. The particle heating time is calculated by solving the energy conservation equation.

$$m_p C_p \frac{dT}{dt} = \dot{q}_{cond} + \dot{q}_{rad}. \quad (5)$$

where m is the mass, C_p the specific heat, and t the time. The rate of conduction heat transfer between the particle and Knudsen layer, \dot{q}_{cond} , is given by [37]

$$\dot{q}_{cond} = \alpha \pi D_p^2 \frac{p_a \sqrt{8k_B T_\beta / \pi m_a}}{8} \left(\frac{\gamma + 1}{\gamma - 1} \right) \left(1 - \frac{T}{T_\beta} \right), \quad (6)$$

where α is the accommodation coefficient, k_B the Boltzmann constant, m_a the mass of ambient gas molecule, γ the specific heat ratio, and T_β is the temperature in the Knudsen layer. Outside the Knudsen layer, the heat transfer rate is calculated using the continuum model [37]

$$\dot{q}_{cond} = 2\pi (D_p + 2\beta) \lambda_a (T_a - T_\beta), \quad (7)$$

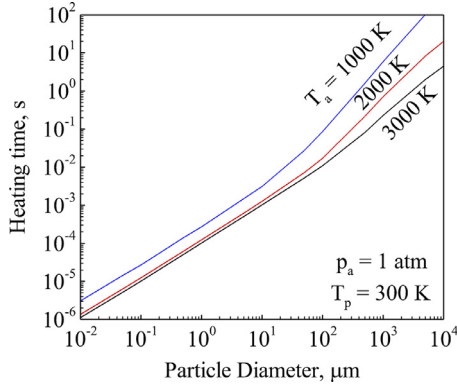


Fig. 8. Effect of particle size on heating time of aluminum particles.

where β is the thickness of the Knudsen layer, which is approximately equal to the mean free path of gas molecules [37]

$$\beta = \frac{3\lambda_a}{\sqrt{\pi} p_a} \frac{\gamma - 1}{9\gamma - 5} \sqrt{\frac{8\pi m_a T_\beta}{k_B}}. \quad (8)$$

The temperature in the Knudsen layer (T_β) is obtained by enforcing the continuity of the heat transfer rate. The thermal conductivity is evaluated at an average temperature, $T^* = (T_a + T_\beta)/2$. Radiation heat transfer rate is calculated using the Stefan-Boltzmann law; the particle emissivity is taken as 0.1. In continuum and free-molecular regimes, the conduction heat transfer rate can be expressed as

$$\dot{q}_{cond} = \alpha \pi D_p^2 \frac{p_a \sqrt{8k_B T_a / \pi m_a}}{8} \left(\frac{\gamma + 1}{\gamma - 1} \right) \left(1 - \frac{T}{T_a} \right), Kn > 10 \quad (9)$$

$$\dot{q}_{cond} = 2\pi D_p \lambda_a (T_a - T), Kn < 0.01 \quad (10)$$

Ignoring the contribution of radiation and integrating Eq. (5), the following closed-form expressions for the particle heating times in continuum and free-molecular regimes are obtained:

$$\tau_{heat} \approx \frac{\rho_p C_p D_p^2}{45\lambda_a}, Kn < 0.01 \quad (11)$$

$$\tau_{heat} \approx \frac{\rho_p C_p}{\alpha p_a} \frac{D_p}{\sqrt{8k_B T_a / \pi m_a}} \left(\frac{\gamma - 1}{\gamma + 1} \right) T_a, Kn > 10 \quad (12)$$

where ρ is the density. Note that it is not possible to obtain closed-form expressions for the characteristic time scales in the transition regime. A numerical analysis of the energy conservation equation is thus employed. Figure 8 shows the effect of particle size on the heating time of aluminum particles. The initial particle temperature is 300 K and the gas pressure is 1 atm. The heating time increases with increasing particle size, from 10 μ s at 100 nm to 10 ms at 100 μ m for a temperature of 3000 K. In the continuum regime, the heating time is quadratically proportional to particle size, while a linear relationship is observed in the free-molecular regime. Furthermore, the heating time is a function of the accommodation coefficient. The accommodation coefficient is the ratio of the actual energy transfer during collision to the counterpart under complete accommodation. Altman [41] proposed the following upper limit for the accommodation coefficient

$$\alpha < \frac{\theta^2}{(2C_v/R + 1)T_a T_p} \quad (13)$$

where $\theta = 428$ K is the Debye temperature of aluminum and C_v the molar specific heat of the gas. The accommodation coefficient is significantly lower than unity, decreasing from about 0.33 at 300 K to 0.03 at 1000 K.

Table 3

Parameters of the polymorphic phase transformation model [4].

| Parameter | Value |
|---------------------------------|--------------------------|
| $E_{\alpha \rightarrow \gamma}$ | 458 kJ/mol |
| $E_{\gamma \rightarrow \alpha}$ | 394 kJ/mol |
| $K_{\alpha \rightarrow \gamma}$ | 10^{12} J/mol/m |
| $K_{\gamma \rightarrow \alpha}$ | 10^8 J/mol/m |
| $F_{\alpha \rightarrow \gamma}$ | 2×10^{15} m/s/K |
| $F_{\gamma \rightarrow \alpha}$ | 5×10^{16} m/s/K |

Note that heating times obtained in this study should be treated as estimates; in some cases, the actual heating times are expected to be lower than the predicted values owing to the effects of radiation heat transfer and chemical reactions preceding ignition of aluminum particles. For example, for an accommodation coefficient of 0.01, the heating time of a 100 nm particle decreases by a factor of about ten when both radiation heat transfer and chemical energy release are considered. The heating time, on the other hand is negligibly affected for accommodation coefficients near unity and for micron-sized particles in the continuum regime.

2.1.3. Mass diffusion vs. polymorphic phase transformations

Particle heating facilitates mass diffusion inside the particle. The diffusion process is promoted by the presence of an electric field in the particle [42]. When an aluminum particle is exposed to the oxidizing gas, gas molecules are adsorbed on the particle surface. Furthermore, metal electrons transverse the oxide layer by thermionic emission or tunneling. These electrons ionize the adsorbed oxidizer molecules to create an electrostatic potential between the metal-oxide and oxide-oxidizer interfaces. The electric field significantly lowers the energy barrier for diffusion. The characteristic time scale for mass diffusion, τ_{diff} , is given by

$$\tau_{diff} \approx \frac{\delta^2}{6D}, \quad (14)$$

where δ is the oxide layer thickness and D the species mass diffusivity. The mass diffusivity is not a well-known parameter. For nano-particles, it falls in the range of 10^{-12} – 10^{-8} m²/s, depending on the temperature and phase of the oxide layer [43, 44].

Polymorphic phase transformations could also be of concern in the first stage. The characteristic time scale of polymorphic phase transformations in the oxide layer, τ_{poly} , is given by

$$\tau_{poly} \approx \frac{\rho_{ox} V_{ox}}{\dot{m}_{ox}^{tr}}, \quad (15)$$

where V is the volume and the subscript *ox* refers to the oxide. The rate of polymorphic transformation of the oxide layer, \dot{m}_{ox}^{tr} , is written as [4]

$$\dot{m}_{ox}^{tr} = \pi D_p^2 \rho_1 F_{x \rightarrow y} T_p \exp\left(-\frac{E_{x \rightarrow y}}{RT_p}\right) \left\{ 1 - \exp\left(-\frac{K_{x \rightarrow y} \delta_x}{RT_p}\right) \right\}, \quad (16)$$

where the subscripts *x* and *y* refer to existing and new polymorphs, respectively. Table 3 lists the parameters of the polymorphic phase transformation model [4]. Figure 9 shows the comparison of the particle heating time with characteristic time scales of mass diffusion and polymorphic phase transformations in the oxide layer. The initial temperature of the particle is 300 K. The diffusion coefficient is taken to be 10^{-11} m²/s based on the results of molecular dynamics (MD) simulations of mass diffusion in 7–12 nm aluminum particles with an oxide layer thickness of 1–2 nm [43]. Note that the diffusion coefficient is a temperature-dependent parameter; it increases from about 10^{-11} m²/s at 600 K to 10^{-8} m²/s at 2000 K. In the first stage, characteristic time scales of polymorphic

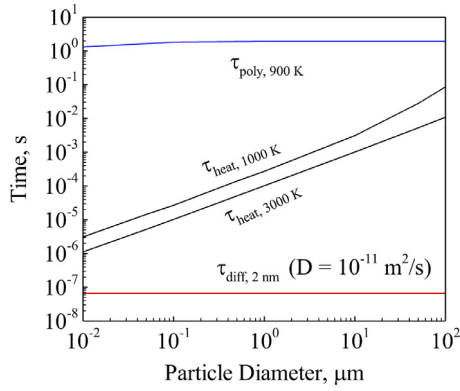


Fig. 9. Comparison of particle heating time with characteristic time scales of mass diffusion and polymorphic phase transformations in the oxide layer.

phase transformations in the oxide layer are orders of magnitude greater than those of heating and mass diffusion. Mass diffusion across the oxide layers of the particles is thus more important in the first stage. Note that the diffusion coefficient used in the analysis corresponds to nano-particles. It is likely that the diffusion coefficient is a size-dependent parameter and it takes a greater value for micron-sized and larger particles. Micron-sized particles, on the other hand, are associated with longer heating times. As a result, mass diffusion is thus expected to be more important than polymorphic phase transformations over the particle size range of concern. Note that empirical correlations [4] and well-established theories [42, 45] are available to treat the heterogeneous oxidation processes prior to ignition.

2.2. Stage II – phase transformations and ignition of nano-aluminum particles

2.2.1. Core melting vs. polymorphic phase transformations in the oxide layer

Melting of the aluminum core marks the beginning of the second stage. The particle energy balance during melting can be written as

$$h_m \frac{dm_l}{dt} = \dot{q}_{cond} + \dot{q}_{rad}, \quad (17)$$

where h_m is the latent heat of melting and T_m the melting temperature. Analytical expressions for the melting time of aluminum particles are obtained as follows:

$$\tau_{melt} \approx \frac{\rho_p h_m D_p^2}{12 \lambda_a (T_a - T_m)}, \quad Kn < 0.01, \quad (18)$$

$$\tau_{melt} \approx \frac{4 \rho_p h_m D_p}{3 \alpha p_a} \frac{T_a}{T_a - T_m} \frac{\gamma - 1}{\gamma + 1} \sqrt{\frac{\pi m_a}{8 k_B T_a}}, \quad Kn > 10. \quad (19)$$

Figure 10 shows the comparison of the time scales of core melting and polymorphic phase transformations in the oxide layer. The oxide layer thickness is taken as 2 nm. At temperatures near the core melting point, time scales of polymorphic phase transformations are substantially greater than those of core melting. As a result, most of the oxide shell is likely to remain amorphous upon melting of the aluminum core. Note that the situation is likely to be different at a different heating rate.

2.2.2. Stresses in the oxide layer

Melting of the aluminum core results in volume dilatation, since the density of liquid aluminum is 2.37 g/cm³, lower than the solid-phase counterpart at the melting point (2.54 g/cm³). This leads to the buildup of compressive and tensile stresses in the core

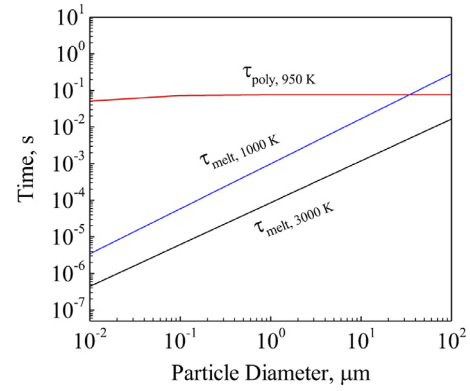


Fig. 10. Comparison of time scales of core melting and polymorphic phase transformations of the oxide layer.

and oxide shell, respectively. The core pressure can be calculated as follows:

$$\Delta p_c = -\Delta \rho_c \frac{K}{\rho_c}, \quad (20)$$

where K is the bulk modulus of bulk aluminum, which is 50 GPa at 933 K [46]. The core pressure is calculated to be 3.35 GPa. The interfacial stresses in the oxide shell can be calculated using the following equations [47]:

$$\sigma_r = -p, \quad (21)$$

$$\sigma_\theta = \sigma_\phi = p \frac{(D_p - 2\delta)^3 + D_p^3/2}{D_p^3 - (D_p - 2\delta)^3}, \quad (22)$$

where σ is the stress. The subscripts r, θ , and ϕ refer to the radial, azimuthal, and polar directions, respectively. The radial stress is calculated to be 3.35 GPa, regardless of the particle size. The polar and azimuthal stresses are substantially greater than the radial counterpart, especially for larger particles. The measured tensile strength of bulk alumina is on the order of 0.1 GPa [24], an order of magnitude lower than the calculated tensile stresses in the oxide layer. The shell is thus likely to fracture for the stress values obtained in this study. Note that the fracture time, t_{frac} , is given by

$$\tau_{frac} \approx \frac{\delta}{V_{crack}}, \quad (23)$$

where V_{crack} is the crack propagation velocity. To a good approximation, the crack speed can be taken as the speed of sound, which is about 10 km/s for bulk alumina [48]. The resulting fracture time is ~ 0.1 ps, substantially lower than the melting time of aluminum particles. Cracking of the oxide layer is thus instantaneous upon melting of the aluminum core.

2.2.3. Cracking vs. mass diffusion

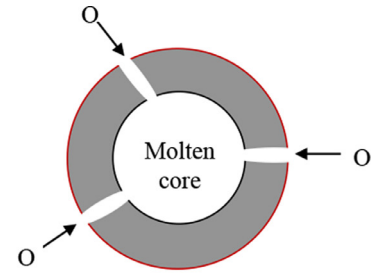
The mechanical properties of oxide shell are not completely understood. Ceramic materials are known typically to be brittle, but deformation is possible for amorphous materials and at high temperatures [49–51]. Firmansyah et al. [52] explored the microstructural behavior of nano-aluminum particles before and after melting of the aluminum core. The particle diameter is 100 nm and oxide layer thickness is 2 nm. High-temperature X-ray diffraction analysis, hot-stage transmission electron microscopy, and high-resolution transmission electron microscopy were employed. When the particle was heated beyond the core melting point, the aluminum core expanded under almost no constraint. Furthermore, the shell fractured with sharp crystalline edges and molten

aluminum flowed out through the cracks. These findings suggest that the amorphous oxide shell is ductile at temperatures near the core melting point and cracking of the oxide layer is aided by polymorphic phase transformations of the oxide shell. Note that the heating rates employed in the study were on the order of 10 °C/min, which facilitated local polymorphic phase transformations of the oxide shell.

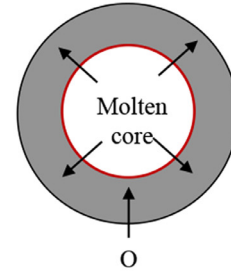
Zhang and Dreizin [53] investigated heterogeneous oxidation of aluminum powders. Thermogravimetric analysis was performed for two sets of powders with nominal size range of 3.0–4.5 and 10–14 μm, respectively. For each powder, the measured weight gain was distributed among particles under the assumption that the oxidation rate is proportional to the reaction surface area. The resulting temporal variations of the particle mass gain obtained from two different powders were compared for a specific particle size. Three different oxidation models were employed, corresponding to ductile and rigid shells and reactions occurring at the core–shell interface and the outer particle surface. Results suggested that reactions occurred at the outer surface of the rigid oxide shell. In a similar study [54], oxidation of aluminum powders in water vapor was characterized by thermogravimetric analysis. The rigid oxide layer fractured multiple times and reactions occurred at the interface or outer surface of the particles. It is apparent that the nature of the oxidizer dictates the integrity of the oxide layer. Note that the heating rate employed in these studies was 5 K/min, orders of magnitude lower than the heating rates of concern to most practical applications (~10⁶ K/s). It is well-known that the mechanical properties of the oxide shell depend on the heating rate, shell thickness, and temperature [55]. Further studies are warranted to understand the properties of the oxide shell at high heating rates.

Puri and Yang [35] conducted MD simulations of the thermo-mechanical behavior of passivated nano-aluminum particles during melting. The heating rate was on the order 10¹³ K/s. The particle size range was 5–10 nm and the oxide layer thickness varied in the range of 1.0–2.5 nm. The oxidation process was characterized by mass diffusion across the oxide layers of the particles. Cracking of the oxide layer was not observed. Similar observations were made by Li et al. [56] and Henz et al. [43] in their MD simulations. The melting temperature of the oxide shell varied in the range of 986–1313 K. These values are substantially lower than the bulk melting point of 2350 K. Results of MD simulations are consistent with the experimental observation that the outward diffusion of aluminum atoms is more significant than inward diffusion of oxidizer molecules [35,43].

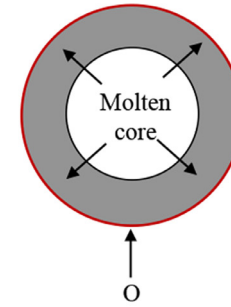
It is apparent that there are three possible burning scenarios for nano-aluminum particles. This is shown in Fig 11. If the oxide layer is rigid and brittle, it fractures due to the tensile stress exerted by the molten aluminum core. The molten aluminum reaches the particle surface by flowing through the cracks/openings in the oxide layer. The ensuing reactions and heat release can result in ignition of nano-aluminum particles due to their low volumetric heat capacity. On the other hand, if the oxide layer is ductile and the pressure is relaxed, particle oxidation will be characterized by mass diffusion across the oxide layer. Depending on diffusion coefficients of aluminum and oxidizer molecules, reactions occur at the core–shell interface or outer surface of the particle. Note that the interfacial oxidation results in new tensile stresses on the oxide layer. The particle mass nearly doubles upon oxidation, while the product density increases only by about 50%. As a result, the oxide layer is under tensile stress and could crack continuously due to geometrical constraints. No such behavior is expected to occur if reactions occur at the outer surface of the particles. Note that the diffusion process speeds up upon melting of the aluminum core and oxide shell. For example, the diffusion coefficient increases by two orders of magnitude, when the temperature increases from



Mode I (Eruptive burning)



Mode II (Interfacial diffusion burning)



Mode III (Surface diffusion burning)

Fig. 11. Three different burning scenarios for nano-aluminum particles: (a) eruptive burning due to fracture of the oxide layer; (b) diffusion burning with reactions at the core–shell interface; (c) diffusion burning with reactions at the particle surface.

600 to 2000 K [43]. This corresponds to a tremendous increase in the oxidation rate of aluminum particles.

2.2.4. Ignition delay

Ignition delay is an important property of concern which can be determined by means of energy balance analysis. The thickness of the oxide layer is taken as 2 nm. The energy conservation equation can be expressed as

$$m_p c_p \frac{dT}{dt} = \dot{q}_{gen} - \dot{q}_{cond} - \dot{q}_{rad} \quad (24)$$

The rate of energy generation, \dot{q}_{gen} , is expressed as

$$\dot{q}_{gen} = \frac{1}{2} \pi D_c^2 \rho_{Al} h_r \frac{dD_c}{dt} \quad (25)$$

where h_r is the heat of reaction. The Mott–Cabrera kinetics has been employed to characterize the oxidation of aluminum particles [42]

$$\frac{dD_p}{dt} = 2(\Omega_1 + \Omega_2) \left(\frac{D_p - 2\delta}{D_p} \right)^2 n \nu \exp\left(\frac{-W}{k_B T}\right) \times \exp\left(\frac{-qa\phi D_p}{k_B T (D_p - 2\delta)\delta}\right) \quad (26)$$

Table 4
Constants in the Mott–Cabrera oxidation model [42].

| Constant | Value |
|------------|--------------------------|
| n | 10 nm^{-2} |
| ν | 10^{12} s^{-1} |
| a | 0.12 nm |
| ϕ_m | -1.6 V |
| W | 2.6 eV |
| q | $3e$ |
| Ω_1 | -0.0166 nm^3 |
| Ω_2 | 0.023 nm^3 |

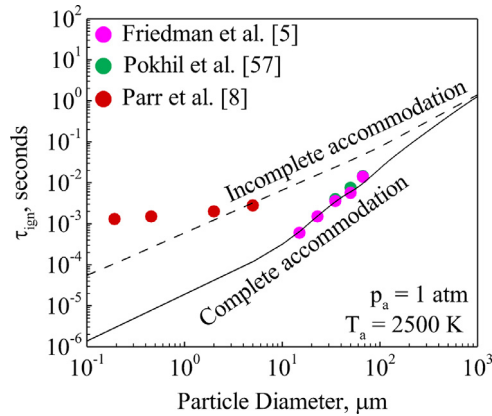


Fig. 12. Effect of particle size on ignition delay of aluminum particles.

$$\frac{d\delta}{dt} = \left[(\Omega_1 + \Omega_2) \left(\frac{D_p - 2\delta}{D_p} \right)^2 - \Omega_1 \right] n\nu \exp\left(\frac{-W}{k_B T}\right) \times \exp\left(\frac{-qa\phi D_p}{k_B T (D_p - 2\delta)\delta}\right), \quad (27)$$

where Ω_1 is the core volume vacated per ion displacement, Ω_2 the volume of the oxide shell formed per displaced ion, n the number of ions per unit area jumping over the energy barrier, W the energy barrier, ν the attempt frequency of the jump, a the distance between the energy barrier maximum and adjacent minimum, and ϕ the Mott potential. Table 4 shows the parameters of the Mott–Cabrera kinetics model.

Ignition delay is defined as the time taken for temperature runaway to occur. Figure 12 shows the effect of particle size on the ignition delay of aluminum particles. The gas temperature is taken to be 2500 K. Model predictions are compared with experimental data. For micron-sized and larger particles, ignition delay is quadratically proportional to the particle size [5,57]. Predictions of the continuum model are in good agreement with experimental data. At nano-scales, particle size exerts a weak effect on the ignition delay. Note that the continuum model significantly underpredicts the ignition delay and overestimates the size dependence of ignition delay of nano-aluminum particles. Better agreement with experimental data is achieved using a free-molecular model and treating the effect of incomplete energy accommodation. In the present analysis, the accommodation coefficient is treated as a size-independent parameter. It is not yet understood how the accommodation coefficient varies with particle size. Furthermore, in the experiments of Parr et al. [8], particles could agglomerate and measured ignition delays may thus correspond to agglomerates as opposed to original particles. These information are necessary to completely understand the size-dependence of ignition properties, especially in the transition regime. Furthermore, the analysis does not address complexities associated with cracking of oxide layer

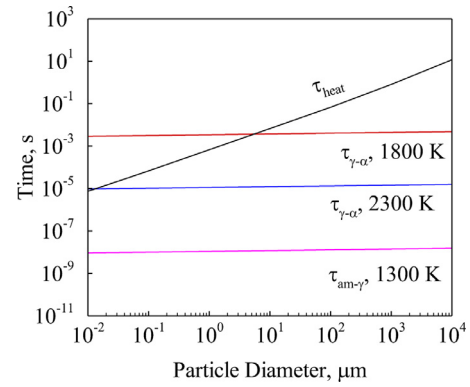


Fig. 13. Comparison of characteristic time scales of heating and polymorphic phase transformations in the oxide layer.

Table 5
Threshold pressure for transition from vapor-phase to surface combustion regime.

| System | Threshold pressure (atm) |
|---|--------------------------|
| Al–CO ₂ (g) | 4.5 |
| Al–H ₂ O (g) | 4.4 |
| Al–H ₂ O (l) | 1.6 |
| Al–H ₂ O (l) ($D_p = 38 \text{ nm}$) | 0.16 |
| Al–air | >100 |

[58] and sintering and agglomeration of particles [59]. These phenomena can be considered in a more advanced model of ignition of aluminum particles. The present analysis provides reasonable estimates of time scales associated with ignition of an isolated aluminum particle using a thermal model based on Mott–Cabrera kinetics. It also offers an explanation for the change in the size dependence of the ignition delay of aluminum particles.

2.3. Stage III – combustion of nanoaluminum particles

In the third stage, nanoaluminum particles react vigorously with the oxidizing gas and an aluminum oxide particle is formed. For micron-sized particles, the particle temperature increases gradually toward the bulk melting temperature of the oxide shell (2350 K). The heating time can be calculated using Eqs. (5)–(8). Figure 13 shows the comparison of particle heating times with characteristic time scales of polymorphic phase transformations in the oxide layer. It is apparent that polymorphic phase transformations in the oxide layer are significant in the third stage and a crystalline alumina layer is formed. The oxide layer melts and ignition of micron-sized and larger aluminum particles is achieved.

2.3.1. Vapor phase vs. surface combustion

The mode of combustion depends on various parameters including the particle size, pressure, and type of oxidizer. The adiabatic flame temperature is typically lower than the boiling point of aluminum for pressures greater than a threshold value. Table 5 shows the threshold pressures for different oxidizers under stoichiometric conditions. Calculations were performed using the NASA chemical equilibrium with applications (CEA) program [60]. The threshold pressure is greater than 100 atm for air and is around 2 and 5 atm for water and carbon dioxide, respectively. Surface reactions are thus more important for water and carbon dioxide environments. Note that the particle size in the nano-scale range may also affect the mode of combustion. For example, the threshold pressure for water is about 0.1 atm for a particle size of 38 nm. This can be attributed to the fact that the inert oxide layer constitutes a greater portion of the particle mass at nano-scales; a

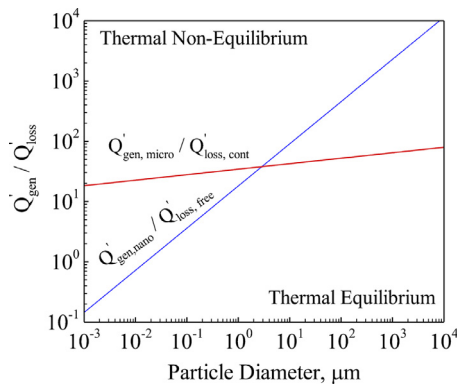


Fig. 14. Comparison of rates of heat generation due to chemical reactions and heat losses to the ambient gas.

38 nm aluminum particle, for example, contains 47 wt% oxide [3]. Combustion of nanoaluminum particles in water and carbon dioxide therefore occur heterogeneously at the particle surface over the pressure range of practical concern (e.g., 1–100 atm).

Results of chemical equilibrium analysis suggest that vapor-phase reactions occur in oxygenated environments for nanoaluminum particles. In the previous analysis, effects of heat losses to the ambient gas were neglected. In reality, the flame temperature is dictated by the competing effects of heat generation due to chemical reactions and heat losses to the ambient gas [61]. Figure 14 shows the comparison of rates of heat generation and heat losses to the ambient gas. Both radiation and conduction heat transfer modes are considered. To facilitate the analysis, the particle is assumed to be heated to a temperature greater than the ambient gas temperature by 200 K due to energy release from chemical reactions. As the continuum model is applicable for micron-sized and larger particles, the corresponding gas temperature is taken to be 2000 K, which roughly correspond to the ignition temperature of micron-sized aluminum particles. For the free-molecular model, the gas temperature is taken to be 1300 K, which is roughly the ignition temperature of nanoparticles. The choice of these temperatures is somewhat arbitrary and does not affect the outcome of the analysis. For simplicity, the characteristic time scale of heat generation is assumed to be equal to the single-particle burning time. If the rate of heat generation is greater than that of heat loss to the ambient gas, the particle could be heated to the boiling point of aluminum ($T_b = 2740$ K at 1 atm), thereby facilitating vapor-phase reactions. This is the case for micron-sized and larger particles. For nanoparticles, heat losses becomes more important and comparable to heat generation. The particle temperature is thus likely to be lower than the adiabatic flame temperature. Note that the above result is not surprising since the surface-to-volume ratio of the particle increases with decreasing particle size. As a result, rate of energy loss to the ambient environment becomes comparable or greater than that of the energy release rate. In the analysis, the accommodation coefficient was about two orders of magnitude lower than unity. Under these conditions, radiation heat transfer becomes more important than the conduction counterpart. The radiation heat transfer rate is independent of pressure, while the heat generation rate is directly proportional to pressure. Deviations from thermal equilibrium conditions thus become significant at higher pressures (> 1 atm). Furthermore, as the heat generation rate is a function of the oxidizer composition, thermal equilibrium conditions are more prevalent for carbon dioxide and water vapor and in dilute oxygenated environments.

Figure 15 shows the effect of particle size on the measured flame temperatures of aluminum particles in oxygenated and carbon dioxide environments. The measurements at 1 atm pressure

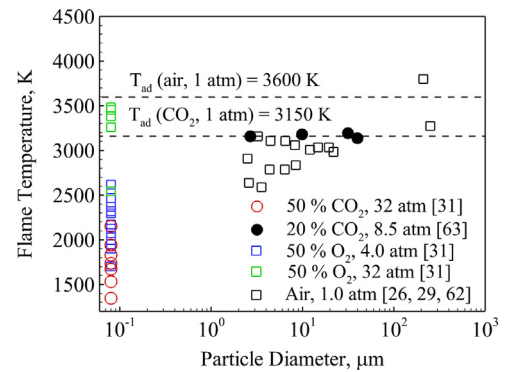


Fig. 15. Measured flame temperature of aluminum particles in different oxidizing gases (adapted from Ref. [6]).

correspond to laser ignited particles [26, 29, 62] and those at higher pressures correspond to particles ignited in a shock tube [31, 63]. The flame temperature was determined by monitoring the intensity of the light emitted by the particles. For micron-sized aluminum particles, the measured flame temperatures are approximately equal to the adiabatic counterparts. At nano-scales, flame temperatures are substantially lower than the adiabatic counterparts over a pressure range of 4–8 atm. This trend is in agreement with the results of the heat transfer analysis. The scatter in the experimental data stems from the fact that the ambient gas temperature was varied in the range of 1200–2100 K. The flame temperature is, however, as high as ~ 3400 K at 32 atm, suggesting that deviations from thermal equilibrium conditions are substantial at a pressure of 32 atm. Note that the boiling temperature of aluminum is also a pressure-dependent parameter and it takes a value of 3800 K at 32 atm. As a result, combustion of nanoaluminum particles occur heterogeneously at the particle surface over the pressure range of concern. This is more so should size dependence of boiling point be considered. Dreizin [64], for example, studied the effect of Laplace pressure on the boiling point of aluminum particles. At 1 atm pressure, the boiling point of 100 nm aluminum particles is ~ 3700 K, substantially greater than the bulk value of 2740 K. Transition from continuum to free-molecular heat transfer regime is yet another factor that drives the flame closer to the particle surface [65].

2.3.2. Mass diffusion vs. chemical kinetics

2.3.2.1. Characteristic time scales. The combustion mechanism of nano-aluminum particles can be determined by comparing the characteristic time scales of mass diffusion and chemical reactions. Note that diffusion can occur through the gas-phase mixture and the oxide layer covering the particle. If mass diffusion through the gas-phase mixture is the rate-controlling process, the burning time of aluminum particles is given by [66,67]

$$t_{b,diff} = \frac{\rho_p D_p^2}{8 \rho_a D_O \log(1 + i Y_{O,a})}, Kn < 0.01 \quad (28)$$

$$t_{b,diff} = \frac{\rho_p D_p}{i p_a Y_{O,a} M_a} \sqrt{\frac{\pi R T_a M_O}{2}}, Kn > 10, \quad (29)$$

where i is the stoichiometric fuel-oxidant mass ratio, Y the mass fraction, and M the molecular weight. The subscript O refers to the oxidizer. In the continuum regime, the burning time is quadratically proportional to the particle size and independent of the gas pressure, since the pressure effects on the density and diffusivity counteract each other. The burning time is however a linear function of the particle size and inversely proportional to gas pressure in the free-molecular regime. The diffusion coefficient of oxygen in

air is given by [68]

$$D_0 = k_1 \left(\frac{T}{T_0} \right)^{k_2} \frac{p_0}{p}, \quad (30)$$

where T is the temperature in Kelvin, p the pressure in atm, T_0 the reference temperature (1 K), and p_0 the reference pressure (1 atm). The constants k_1 and k_2 are $1.13 \times 10^{-9} \text{ m}^2/\text{s}$ and 1.724, respectively. The resulting burning times of 100 nm aluminum particles vary in the range of 10^{-7} – 10^{-5} s at a pressure of 1 atm.

If mass diffusion inside the particle is the rate-controlling step, the particle burning time can be expressed as

$$t_{b,diff} \approx \frac{R_p^2}{6D}, \quad (31)$$

where D is the mass diffusion coefficient in the particle. If particle combustion is limited by chemical kinetics, the burning time is given by [66]

$$t_{b,chem} = \frac{\rho_p D_p}{2M_p k p_a X_{O,a}}, \quad (32)$$

where k is the rate constant and X the mole fraction. The resulting burning times are strongly dependent on temperature, since rate constants for chemical reactions and mass diffusion are exponential functions of temperature.

The diffusion coefficient and chemical rate constants are poorly known parameters. Henz et al. [43] conducted MD simulations of mechanochemical behaviors of nano-aluminum particles of diameters 5.6 and 8.0 nm. Two different oxide layer thicknesses of 1 and 2 nm were considered. The mass diffusivity in the oxide layer was on the order of 10^{-9} – $10^{-7} \text{ m}^2/\text{s}$ over the temperature range of 1000–2000 K. Substituting these values in Eq. (31), the burning time of 100 nm particles is estimated to be 10^{-9} – 10^{-7} s. Note, however, that diffusion coefficients obtained using MD simulations correspond to particles with diameters lower than 10 nm. Park et al. [33] studied the oxidation of 50–150 nm aluminum particles using a single particle mass spectrometer (SPMS) for temperatures up to 1373 K. The diffusion coefficient was estimated to be on the order of 10^{-13} – $10^{-12} \text{ m}^2/\text{s}$ over a temperature range of 873–1173 K. Extrapolating these values to a higher temperature of 2000 K, the diffusion coefficient is obtained as $10^{-11} \text{ m}^2/\text{s}$. The resulting burning time is on the order of 10^{-5} s.

2.3.2.2. Comparison with experimental data. The combustion mechanism of nano-aluminum particles can be determined by comparing the measured and calculated burning times. The dependence of burning time on particle size, pressure, and temperature can be used to gain insight on the combustion mechanism. Figure 16

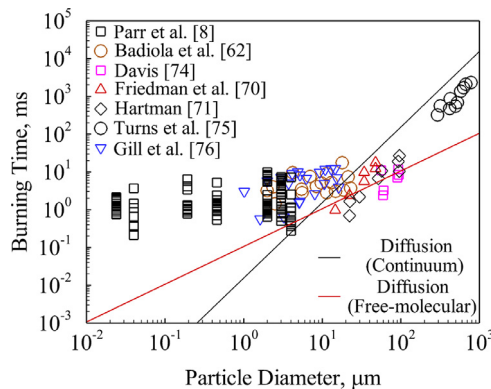


Fig. 16. Comparison of measured burning times of aluminum particles with theoretical counterparts under diffusion-controlled conditions.

shows the comparison of measured burning times with theoretical counterparts under diffusion-controlled conditions. Experimental data on measured burning times of aluminum particles are available in Refs. [8, 62,69–76]. For nano-aluminum particles, the calculated gas-phase diffusion times are several orders of magnitude lower than the measured burning times for nano-aluminum particles. As a result, mass diffusion through the gas-phase mixture does not control the burning rate of nano-aluminum particles.

As the chemical rate constant and mass diffusion coefficient in the oxide layer are poorly known parameters, comparison of characteristic time scales of mass diffusion and chemical kinetics is not possible. It is however apparent from Fig. 16 that particle size exerts a weak effect on the burning time of nano-aluminum particles. The burning time has a size dependence of the form $\tau_b = aD_p^n$, where the exponent n is ~ 0.3 [6]. The diameter exponent is lower than unity due to the presence of cracks in the oxide layer [58] and/or sintering and agglomeration of particles [59]. The cracks in the oxide layer increase the fractal dimension of the particle surface, while the particle volume is negligibly affected. The resulting diameter exponent is significantly lower than unity under kinetically-controlled conditions. Moreover, particles tend to aggregate during combustion and the resulting burning time may not correspond to the initial particle size. Furthermore, gas pressure and temperature exert strong effects on burning time of nanoaluminum particles. The burning time is an exponential function of temperature, with activation energies in the range of 50–144 kJ/mol [6]. It decreases by a factor of four when the pressure increases from 8 to 32 atm [31]. Note that, in the free-molecular regime, gas-phase diffusion time scale is proportional to the square-root of temperature, whereas time scales of mass diffusion through the oxide layer and chemical kinetics are exponential functions of temperature. These, together with the observed size dependence of burning time, not only substantiate the fact that mass diffusion through the gas-phase mixture is not the rate-controlling process, but also suggest the burning rate of nano-aluminum particles is controlled by chemical kinetics. Note that the chemical rate constant is a poorly known parameter and needs further investigation. Furthermore, several important phenomena such as sintering and agglomeration of particles and cracking of the oxide layer must be considered before a comparison can be drawn between predictions and experimental data. These phenomena can be considered in a future work to develop a rigorous model of combustion of nano-aluminum particles.

2.4. Stage IV – combustion of large micron-sized aluminum particles

The fourth stage involves combustion of large micron-sized particles. As discussed in Section 2.3, vapor-phase combustion is expected in oxygenated environments, while surface reactions are more important for water vapor and carbon dioxide oxidizers, especially at higher pressures. It is apparent from Figs. 14 and 15 that the flame temperatures are approximately equal to the adiabatic counterparts. For a particle burning under diffusion-controlled conditions, the burning time is given by

$$t_{b,diff} = \frac{\rho_p D_p^2}{8\rho_a D_0 \log(1+B)}. \quad (33)$$

The transfer number is given by

$$\text{Vapor – phase combustion : } B = \frac{iY_{O,a}H_R + C_p(T_a - T_p)}{L_v}, \quad (34)$$

$$\text{Surface combustion : } B = iY_{O,a}. \quad (35)$$

Note that these time scales should be treated as estimates rather than being accurate representation of the particle burning time. As evident from Fig. 16, the measured burning times

Table 6
Modes of ignition of aluminum particles.

| Length scales | | Shell type | Ignition mechanism |
|---------------|------------|----------------|---|
| Core | Shell | | |
| Nano | Thick | Rigid/brittle | Fracture due to core melting and/or polymorphic phase changes |
| | Thin | Rigid/brittle | Fracture, melting, and polymorphic phase changes of the oxide shell |
| Nano | Thick | Flexible | Mass diffusion across oxide layer and polymorphic phase changes |
| | Thin | Flexible | Melting of oxide shell and polymorphic phase changes |
| Large micron | Thick/thin | Rigid/flexible | Melting of oxide shell |

Table 7
Modes and mechanisms of oxidation of aluminum particles.

| D_p | T | p | Oxidizer | Primary reaction mode | Rate controlling mechanism |
|--------------|---------------|------|-------------------|---|--|
| Nano, micron | $T < T_{ign}$ | – | O_2, H_2O, CO_2 | Heterogeneous | Mass diffusion across oxide layer |
| Nano | | – | O_2, H_2O, CO_2 | Surface (Heterogeneous) | Chemical kinetics |
| Small micron | $T > T_{ign}$ | Low | O_2, H_2O, CO_2 | Vapor-phase (Homogeneous) and surface (Heterogeneous) | Mass diffusion through the gas-phase mixture and chemical kinetics |
| | | High | O_2 | Vapor-phase (Homogeneous) and surface (Heterogeneous) | |
| Large micron | | Low | H_2O, CO_2 | Surface (Heterogeneous) | Mass diffusion through the gas-phase mixture |
| | | | O_2, H_2O, CO_2 | Vapor-phase (Homogeneous) | |
| | | | O_2 | Vapor-phase (Homogeneous) | |
| | | High | H_2O, CO_2 | Surface (Heterogeneous) | |

are in reasonably good agreement with theoretical counterparts under diffusion-controlled conditions. Furthermore, experimental data suggests that the burning time is weakly dependent on the pressure and temperature of the ambient gas [77]. These corroborate the fact that the burning rate of large micron-sized aluminum particles is limited by mass diffusion through the gas-phase mixture.

2.5. Modes of ignition and combustion of aluminum particles

The ignition and combustion mechanisms of aluminum particles depend on various parameters including the particle size, oxide layer thickness, oxidizer, pressure, and temperature. Table 6 shows different modes of ignition of aluminum particles. For nanoparticles with thick, rigid, and brittle oxide layers, ignition is caused by the fracture of the oxide layer. The oxide layer cracks due to the tensile stress exerted by the molten aluminum core. Furthermore, polymorphic phase transformations can result in openings in the oxide layer. The cracks/openings provide pathways for the aluminum particle to react with the oxidizing gas. The ensuing heat release facilitates the ignition of small particles due to their low volumetric heat capacity. For nanoparticles with thin oxide layers, ignition could also be triggered by melting of the oxide shell. The melting temperature of the oxide shell is a function of the shell thickness; it takes a value as low as ~ 1000 K for a shell thickness of 1 nm [78]. Melting promotes mass diffusion across the oxide layer, thereby facilitating particle ignition. For particles with flexible oxide layers, the core pressure is relaxed upon melting due to unrestrained expansion. As a result, ignition is caused by mass diffusion across the oxide layers of the particles and polymorphic phase transformations. For large micron-sized particles with high volumetric heat capacities, ignition is achieved only upon melting of the oxide layer.

The oxidation behavior of aluminum particles depends on the particle size, oxidizer, pressure, and temperature. Table 7 shows the oxidization scenarios of aluminum particles. For all cases, reactions preceding ignition occur heterogeneously at the particle surface. The oxidation rate is controlled by mass diffusion across the oxide layers of particles. For nanoparticles, combustion is characterized by heterogeneous surface reactions and the burning rate is dictated by chemical kinetics. For large micron-sized particles,

the mode of combustion depends on the gas pressure and type of oxidizer. Vapor-phase reactions occur in oxygenated environments, while surface reactions are important for water vapor and carbon dioxide, especially at high pressures. The particle burning rate is controlled by mass diffusion through the gas-phase mixture. For particles in the intermediate size range, both vapor-phase and surface reactions are important and the burning rate is controlled by chemical kinetics and mass diffusion through the gas-phase mixture.

3. Conclusions

A general theory of ignition and combustion of nano- and micron-sized aluminum particles was proposed. The oxidation process was divided into different stages based on phase transformations and chemical reactions. Characteristic time scales of different processes were compared to identify physicochemical phenomena in each stage. In the first stage, the particle was heated to the melting temperature of the aluminum core. Key processes were heat and mass transfer between the gas and particle surface and diffusion of mass and energy inside the particle. The second stage began upon melting of the aluminum core. Melting resulted in pressure buildup and facilitated outward motion of molten aluminum by diffusion and/or flow through the cracks in the oxide layer. Melting was followed by polymorphic phase transformations in the oxide layer. If the oxide layer was rigid and brittle, it fractures due to the tensile stress exerted by the molten aluminum core, thereby igniting the nanoparticle. On the other hand, if the oxide layer is flexible/ductile and the pressure is relaxed, particle oxidation will be characterized by mass diffusion across the oxide layer. Depending on diffusion coefficients of aluminum and oxidizer molecules, reactions occur at the core-shell interface or outer surface of the particle. For nanoparticles with thin oxide layers, melting of the oxide layer could also be of concern to ignition. Furthermore, polymorphic phase transformations could assist in ignition of nanoparticles due to creation of openings in the oxide layer due to differences in densities of oxide polymorphs. For large micron-sized particles, ignition was not achieved possibly due to their greater volumetric heat capacity. In the third stage, nanoparticles underwent vigorous self-sustaining reactions with the oxidizing gas. Reactions occurred heterogeneously inside

the particle and/or on the particle surface. Experimental data suggested that the burning time of nanoparticles is weakly dependent on particle size, but strongly dependent on pressure and temperature of the ambient gas. Comparison of characteristic time scales and evaluation of functional dependence of burning time on particle size, pressure, and temperature suggested that the burning rate of nanoparticles was controlled by chemical kinetics and not mass diffusion processes. For large micron-sized particles, polymorphic phase transformations resulted in the formation of a crystalline oxide layer. Melting of the oxide layer resulted in particle ignition. In the fourth stage, the large micron-sized particle burned through gas-phase or surface reactions, depending on the oxidizer and pressure. The burning rate was controlled by mass diffusion through the gas-phase mixture.

Acknowledgments

This work was sponsored by the Air Force Office of Scientific Research under Contract no. FA-9550-13-1-0004. The support and encouragement provided by Dr. Mitat A. Birkan is gratefully acknowledged.

References

- [1] V. Yang, T.B. Brill, W.Z. Ren, Solid propellant chemistry, combustion, and motor interior ballistics, American Institute of Aeronautics and Astronautics, 2000.
- [2] D.S. Sundaram, P. Puri, V. Yang, Pyrophoricity of nascent and passivated aluminum particles at nano-scales, *Combust. Flame* 160 (2013) 1870–1875.
- [3] G.A. Risha, S.F. Son, R.A. Yetter, V. Yang, B.C. Tappan, Combustion of nano-aluminum and liquid water, *Proce. Combust. Inst.* 31 (2) (2007) 2029–2036.
- [4] M.A. Trunov, M. Schoenitz, E.L. Dreizin, Effect of polymorphic phase transformations in alumina layer on ignition of aluminum particles, *Combust. Theory Model.* 10 (4) (2006) 603–623.
- [5] R. Friedman, A. Maček, Ignition and combustion of aluminum particles in hot ambient gases, *Combust. Flame* 6 (1962) 9–19.
- [6] D.S. Sundaram, V. Yang, Combustion of nano aluminum particles, *Combust. Explos. Shock Waves* 51 (2015) 173–196.
- [7] C. Brossard, A. Ulas, C.L. Yeh, K.K. Kuo, Ignition and combustion of isolated aluminum particles in the post-flame region of a flat-flame burner, 16th International Colloquium on the Dynamics of Explosions and Reactive Systems, Krakow, Poland (1997).
- [8] T. Parr, C. Johnson, D. Hanson-Parr, K. Higa, K. Wilson, Evaluation of advanced fuels for underwater propulsion, JANNAF Combustion Subcommittee Meeting (2003).
- [9] I.G. Assovskiy, O.M. Zhigalina, V.I. Kolesnikov-Svinarev, Gravity effect in aluminum droplet ignition and combustion, Fifth International Microgravity Combustion Workshop Cleveland, USA, 1999, Cleveland, USA (1999).
- [10] C.J. Bulian, T.T. Kerr, J.A. Puszyński, Ignition studies of aluminum and metal oxide nanopowders, 31st International Pyrotechnics Seminar, Fort Collins, Colorado (2004).
- [11] M.E. Derevyga, L.N. Stesik, E.A. Fedorin, Studies on ignition and combustion of aluminum and zinc in air, *Combust. Explos. Shock Waves* 13 (1977) 722–726.
- [12] V.A. Ermakov, A.A. Razdobreev, A.I. Skorik, V.V. Pozdeev, S.S. Smolyakov, Temperature of aluminum particles at the time of ignition and combustion, *Combust. Explos. Shock Waves* 18 (2) (1982) 256–257.
- [13] D.K. Kuehl, Ignition and combustion of aluminum and beryllium, *AIAA J.* 3 (1965) 2239–2247.
- [14] S. Yuasa, Y. Zhu, S. Sogo, Ignition and combustion of aluminum in oxygen/nitrogen mixture streams, *Combust. Flame* 108 (1997) 387–390.
- [15] M.A. Gurevich, K.I. Lapkina, E.S. Ozerov, Ignition limits of aluminum particles, *Combust. Explos. Shock Waves* 6 (2) (1970) 154–157.
- [16] M. Schoenitz, C. Chen, E.L. Dreizin, Oxidation of aluminum particles in the presence of water, *J. Phys. Chem. B* 113 (15) (2009) 5136–5140.
- [17] T.G. Theofanous, X. Chen, P. Di Piazza, M. Epstein, H.K. Fauske, Ignition of aluminum droplets behind shock waves in water, *Phys. Fluids* 6 (1994) 3513–3515.
- [18] A.F. Belyaev, Y.V. Frolov, A.I. Korotkov, Combustion and ignition of particles of finely dispersed aluminum, *Combust. Explos. Shock Waves* 4 (3) (1968) 182–185.
- [19] V.A. Fedoseev, Burning of magnesium and aluminum particles in various media, *Fiz. Aerodispersnykh Sist.* 3 (1970) 61.
- [20] A.G. Alekseev, R.A. Barlas, T.I. Tsidelko, A.F. Shapoval, Effect of particle size on the combustibility and explosion parameters of dispersed aluminum and magnesium powders, *Preduprezhdenie Vnezapnykh Vzryvov Gazodispersnykh Sistem*, V.V. Nedin, (Ed.) 1971; p 66.
- [21] A.G. Merzhanov, Y.M. Grigorjev, Y.A. Galchenko, Aluminum ignition, *Combust. Flame* 29 (1977) 1.
- [22] B.I. Khaikin, B.N. Bloshenko, A.G. Merzhanov, On the ignition of metal particles, *Combust. Explos. Shock Waves* 6 (4) (1970) 474–488.
- [23] A. Rai, D. Lee, K. Park, M.R. Zachariah, Importance of phase change of aluminum in oxidation of aluminum nanoparticles, *J. Phys. Chem. B* 108 (39) (2004) 14793–14795.
- [24] J.F. Shackelford, W. Alexander, CRC materials science and engineering handbook, CRC Press, 2000.
- [25] P. Bucher, R.A. Yetter, F.L. Dryer, T. Parr, D.M. Hanson-Parr, PLIF species and radiometric temperature measurements of aluminum particle combustion in O₂, CO₂ and N₂O oxidizers, and comparison with model calculations, *Symp. (Int.) Combust.* 27 (2) (1998) 2421–2429.
- [26] E.L. Dreizin, On the mechanism of asymmetric aluminum particle combustion, *Combust. Flame* 117 (1999) 841–850.
- [27] P. Bucher, R.A. Yetter, F.L. Dryer, T.P. Parr, D.M. Hanson-Parr, E.P. Viceni, Flames structure measurement of single, isolated aluminum particles burning in air, *Symp. (Int.) Combust.* 26 (2) (1996) 1899–1908.
- [28] E.L. Dreizin, Experimental study of stages in aluminum particle combustion in air, *Combust. Flame* 105 (4) (1996) 541–556.
- [29] R.A. Yetter, F.L. Dryer, Micro gravity combustion: fire in free fall, in: H.D. Ross (Ed.), Academic Press, 2001.
- [30] M.W. Beckstead, Correlating aluminum burning times, *Combust. Explos. Shock Waves* 41 (5) (2005) 533–546.
- [31] T. Bazyn, H. Krier, N. Glumac, Combustion of nanoaluminum at elevated pressure and temperature behind reflected shock waves, *Combust. Flame* 145 (4) (2006) 703–713.
- [32] Y. Huang, G.A. Risha, V. Yang, R.A. Yetter, Effect of particle size on combustion of aluminum particle dust in air, *Combust. Flame* 156 (1) (2009) 5–13.
- [33] K. Park, D. Lee, A. Rai, D. Mukherjee, M.R. Zachariah, Size-resolved kinetic measurements of aluminum nanoparticle oxidation with single particle mass spectrometry, *J. Phys. Chem. B* 109 (15) (2005) 7290–7299.
- [34] P. Puri, V. Yang, Effect of particle size on melting of aluminum at nano scales, *J. Phys. Chem. C* 111 (32) (2007) 11776–11783.
- [35] P. Puri, V. Yang, Thermo-mechanical behavior of nano aluminum particles with oxide layers during melting, *J. Nanopart. Res.* 12 (8) (2010) 2989–3002.
- [36] S.W. Chung, E.A. Gulians, C.E. Bunker, P.A. Jelliss, S.W. Buckner, Size-dependent nanoparticle reaction enthalpy: oxidation of aluminum nanoparticles, *J. Phys. Chem. Solids* 72 (6) (2011) 719–724.
- [37] S. Mohan, M.A. Trunov, E.L. Dreizin, Heating and ignition of metal particles in the transition heat transfer regime, *J. Heat Transf.* 130 (10) (2008) 104505-1-104505-5.
- [38] F.P. Incropera, D.P. Dewitt, Fundamentals of heat transfer, John Wiley & Sons, 1981.
- [39] A.V. Filippov, D.E. Rosner, Energy transfer between an aerosol particle and gas at high temperature ratios in the Knudsen transition regime, *Int. J. Heat Mass Transf.* 43 (1) (2000) 127–138.
- [40] N.A. Fuchs, On the stationary charge distribution on aerosol particles in a bipolar ionic atmosphere, *Geofis. Pura Appl.* 56 (1963) 185–193.
- [41] I. Altman, On heat transfer between nanoparticles and gas at high temperatures, *J. Aerosol Sci.* 30 (1999) S423–S424.
- [42] A. Ermoline, E.L. Dreizin, Equations for the Cabrera–Mott kinetics of oxidation for spherical nanoparticles, *Chem. Phys. Lett.* 505 (1–3) (2011) 47–50.
- [43] B.J. Henz, T. Hawa, M.R. Zachariah, On the role of built-in electric fields on the ignition of oxide coated nanoaluminum: Ion mobility versus Fickian diffusion, *J. Appl. Phys.* 107 (2) (2010) 024901-024901-9.
- [44] T. Campbell, R.K. Kalia, A. Nakano, P. Vashishta, Dynamics of oxidation of aluminum nanoclusters using variable charge molecular-dynamics simulations on parallel computers, *Phys. Rev. Lett.* 82 (24) (1999) 4866–4869.
- [45] A.V. Federov, Y.V. Kharlamova, Ignition of an aluminum particle, *Combust. Explos. Shock Waves* 39 (5) (2003) 544–547.
- [46] A.F. Chebanov, Determination of the temperature dependence of the bulk modulus of elasticity of certain pure metals, *Sov. Mater. Sci.* 27 (1992) 184–188.
- [47] A. Ragab, S.E. Bayoumi, Engineering solid mechanics: fundamentals and applications, CRC Press, New York, 1999.
- [48] R.G. Munro, Evaluated material properties for a sintered alpha-alumina, *J. Am. Ceram. Soc.* 80 (1997) 1919–1928.
- [49] G.T. Murray, C.V. White, W. Weise, Introduction to engineering materials: behavior, properties, and selection, Marcel Dekker, New York, 1993.
- [50] C.B. Carter, M.G. Norton, Ceramic materials: science and engineering, Springer, 2013.
- [51] R. Srinivasan, Engineering materials and metallurgy, Tata McGraw Hill, 2010.
- [52] D. Firmansyah, K. Sullivan, K. Lee, Y. Kim, R. Zahaf, M. Zachariah, D. Lee, Microstructural behavior of the alumina shell and aluminum core before and after melting of aluminum nanoparticles, *J. Phys. Chem. C* 116 (1) (2012) 404–411.
- [53] S. Zhang, E.L. Dreizin, Reaction interface for heterogeneous oxidation of aluminum powders, *J. Phys. Chem. C* 117 (2013) 14025–14031.
- [54] H. Nie, S. Zhang, M. Schoenitz, E.L. Dreizin, Reaction interface between aluminum and water, *Int. J. Hydrogen Energy* 38 (2013) 11222–11232.
- [55] V.I. Levitas, B.W. Asay, S.F. Son, M. Pantoya, Mechanochemical mechanism for fast reaction of metastable intermolecular composites based on dispersion of liquid metal, *J. Appl. Phys.* 101 (8) (2007) 083524-083524-20.
- [56] Y. Li, R.K. Kalia, A. Nakano, P. Vashishta, Size effect on the oxidation of aluminum nanoparticle: multimillion-atom reactive molecular dynamics simulations, *J. Appl. Phys.* 114 (2013) 134312.
- [57] P.F. Pokhil, A.F. Belyaev, Y.V. Frolov, Combustion of powdered metals in active media, Science, 1972 Moscow.
- [58] J. Buckmaster, T.L. Jackson, An examination of the shrinking-core model of sub-micron aluminum combustion, *Combust. Theory Model.* 17 (2013) 335–353.

- [59] P. Chakraborty, M.R. Zachariah, Do nanoenergetic particles remain nano-sized during combustion? *Combust. Flame* 161 (2014) 1408–1416.
- [60] B.J. McBride, S. Gordon, Chemical equilibrium with applications (CEA) program, National Aeronautics and Space Administration, 1996.
- [61] D. Allen, H. Krier, N. Glumac, Heat transfer effects in nano-aluminum combustion at high temperatures, *Combust. Flame* 161 (2014) 295–302.
- [62] C. Badiola, R.J. Gill, E.L. Dreizin, Combustion characteristics of micron-sized aluminum particles in oxygenated environments, *Combust. Flame* 158 (10) (2011) 2064–2070.
- [63] T. Bazyn, H. Krier, N. Glumac, Evidence for the transition from the diffusion-limit in aluminum particle combustion, *Proce. Combust. Inst.* 31 (2) (2007) 2021–2028.
- [64] E.L. Dreizin, Effect of surface tension on the temperature of burning metal droplets, *Combust. Flame* 161 (12) (2014) 3263–3266.
- [65] S. Mohan, M.A. Trunov, E.L. Dreizin, On possibility of vapor-phase combustion for fine aluminum particles, *Combust. Flame* 156 (11) (2009) 2213–2216.
- [66] R.A. Yetter, G.A. Risha, S.F. Son, Metal particle combustion and nanotechnology, *Proc. Combust. Inst.* 32 (2) (2009) 1819–1838.
- [67] A. Ermoline, D. Yildiz, E.L. Dreizin, Model of heterogeneous combustion of small particles, *Combust. Flame* 160 (2013) 2982–2989.
- [68] T.R. Marrero, E.A. Mason, Gaseous diffusion coefficients, *J. Phys. Chem. Ref. Data* 1 (1972) 3–118.
- [69] R.P. Wilson, F.A. Williams, Experimental study of the combustion of single aluminum particles in O₂/Ar, *Symp. (Int.) Combust.* 13 (1) (1971) 833–845.
- [70] R. Friedman, A. Mačėk, Combustion studies of single aluminum particles, *Symp. (Int.) Combust.* 9 (1) (1963) 703–712.
- [71] K.O. Hartman, Ignition and combustion of aluminum particles in propellant flame gases, 8th JANNAF Combustion Meeting (1971).
- [72] S.E. Olsen, M.W. Beckstead, Burn time measurements of single aluminum particles in steam and CO₂ mixtures, *J. Propuls. Power* 12 (4) (1996) 662–671.
- [73] J. Prentice, Combustion of laser-ignited aluminum droplets in wet and dry oxidizers, 12th Aerospace Sciences Meeting (1974).
- [74] A. Davis, Solid propellants: the combustion of particles of metal ingredients, *Combust. Flame* 7 (1963) 359–367.
- [75] S.R. Turns, S.C. Wong, E. Ryba, Combustion of aluminum-based slurry agglomerates, *Combust. Sci. Technol.* 54 (1987) 299–318.
- [76] R.J. Gill, C. Badiola, E.L. Dreizin, Combustion times and emission profiles of micron-sized aluminum particles burning in different environments, *Combust. Flame* 157 (2010) 2015–2023.
- [77] M. Marion, C. Chauveau, I. Gokalp, Studies on the ignition and burning of levitated aluminum particles, *Combust. Sci. Technol.* 115 (1996) 369–390.
- [78] E.L. Dreizin, D.J. Allen, N.G. Glumac, Depression of melting point for protective aluminum oxide films, *Chem. Phys. Lett.* 618 (2015) 63–65.